

Out-of-Plane Nonlinear Orbital Hall Torque

Hui Wang,^{1,*} Xukun Feng,^{2,*} Jin Cao,³ Huiying Liu,⁴ Weibo Gao,^{5,6,7} Cong Xiao,^{2,†} Shengyuan A. Yang,^{3,‡} and Lay Kee Ang^{1,§}

¹*Science, Mathematics and Technology (SMT), Singapore University of Technology and Design, Singapore 487372, Singapore*

²*Interdisciplinary Center for Theoretical Physics and Information Sciences (ICTPIS), Fudan University, Shanghai 200433, China*

³*Research Laboratory for Quantum Materials, Department of Applied Physics, The Hong Kong Polytechnic University, Kowloon, Hong Kong SAR, China*

⁴*School of Physics, Beihang University, Beijing 100191, China*

⁵*Division of Physics and Applied Physics, School of Physical and Mathematical Sciences, Nanyang Technological University, Singapore 637371, Singapore*

⁶*School of Electrical and Electronic Engineering, Nanyang Technological University, Singapore*

⁷*Centre for Quantum Technologies, National University of Singapore, Singapore*

Despite recent advances in orbitronics, generating out-of-plane orbital torques essential for field-free deterministic switching of perpendicular magnetization remains a key challenge. Here, we propose a strategy to produce such unconventional torques across broad classes of materials, by leveraging the nonlinear orbital Hall effect. We demonstrate that this nonlinear orbital response is dramatically amplified by topological band degeneracies, where it overwhelmingly dominates the spin response even in systems with strong spin-orbit coupling. These features are confirmed via a quantitative investigation of representative topological metals RhSi, YPtBi, and PbTaSe₂, by combining our theory with first-principles calculations. The resulting orbital torques substantially surpass those from linear mechanisms reported thus far. These findings propel the research of orbital transport into the nonlinear regime, broaden the scope of orbital source materials, and establish a new pathway towards high-performance orbitronic devices.

Orbital Hall effect, which generates a transverse flow of orbital angular momentum by an applied electric current, has been a focus of recent research [1–14]. As a potential application, its produced orbital current can be injected into a neighboring magnetic layer and exert a torque on the magnetization. This orbital Hall torque offers an electric means to induce magnetic dynamics or even achieve magnetic switching [11, 15–18]. Recent studies have demonstrated strong orbital Hall effect generated by light elemental transition metals [11, 12], in which the driving charge current, generated orbital current and its orbital polarization are mutually orthogonal. Unfortunately, this type of orbital current is inefficient for manipulating magnets with perpendicular magnetic anisotropy (PMA), which are a key element for high-density scalable magnetic memory devices [19–24].

The torque required to achieve field-free deterministic switching of PMA magnets should be out-of-plane, which arises from an unconventional collinearly-polarized (CP) component of orbital Hall current j_a^p , namely, the flow direction a and the orbital polarization direction p should be the same [20, 24]. However, such CP orbital current is forbidden by the high crystalline symmetry in the most studied orbital Hall materials, like Ti and Cr [7, 11, 12]. This has posed a critical challenge for the development of orbitronics.

In this work, we propose a strategy for generating CP orbital currents across broad classes of materials, by exploiting a new physical effect: the nonlinear orbital Hall effect (NOHE). Here, ‘nonlinear’ means the generated orbital current is quadratic in the driving electric field,

$j_a^p \propto E^2$. We show that NOHE is far less constrained for producing CP orbital currents: it is permitted in 19 out of the 21 noncentrosymmetric crystal classes. Notably, in 9 of these classes, the linear CP orbital Hall response is entirely forbidden. These nine classes encompass numerous topological materials of recent interest, such as chiral multifold fermion semimetals and half-Heusler topological semimetals. We develop the theory for NOHE, with both intrinsic and extrinsic mechanisms. We show that the intrinsic NOHE is significantly amplified by topological band crossing features, where the orbital response dominates over the spin response. These points are confirmed by quantitative evaluation in concrete topological metals: RhSi, YPtBi, and PbTaSe₂, by combining our theory with first-principles calculations. Furthermore, we uncover that (i) the out-of-plane torque efficiency from NOHE can surpass that of previously reported linear mechanisms; (ii) while current orbitronic research mainly focuses on light materials with weak spin-orbit coupling (SOC), NOHE is highly sensitive to band topology and can prevail over spin responses even in strong-SOC systems; and (iii) the sign of the NOHE-induced orbital torque can be well controlled via crystal symmetry. Our findings unveil NOHE as a new physical effect, open a new avenue of research for orbitronics, and provide a pathway to overcome the challenges in generating out-of-plane orbital torques.

CP nonlinear orbital Hall current. The orbital current

j_a^p induced by nonlinear response can be expressed as

$$j_a^p = \sum_{b,c} \chi_{abc}^p E_b E_c. \quad (1)$$

The nonlinear orbital conductivity tensor χ_{abc}^p is a time-reversal-even rank-4 pseudo-tensor for nonmagnetic materials, and requires broken inversion symmetry. We are interested in the CP current from NOHE, which corresponds to χ components with $p = a \neq b, c$. From symmetry analysis, we find that the CP NOHE response is permitted in 19 out of the 21 noncentrosymmetric crystal classes. Particularly, in 9 of these classes, including C_{2v} , D_2 , D_4 , D_6 , D_{2d} , D_{3h} , T_d , T , and O , NOHE provides the leading-order contribution, since the linear CP orbital current is symmetry forbidden (details in Supplementary Note 1). We shall choose three representative material examples for concrete studies, which belong to T (RhSi), T_d (YPtBi), and D_{3h} (PbTaSe₂). The symmetry allowed components $\chi_{a(bc)}^a$ ($\equiv (\chi_{abc}^a + \chi_{acb}^a)/2$) for these 3 classes are listed in Table I.

Comparison with spin current response. The orbital current response is always accompanied by a spin counterpart, since the two share the same symmetry. Before detailed evaluation, one can actually get some qualitative understanding, especially on their relative strength.

The orbital and spin current operators can be expressed as [25] $\hat{j}_a^p = \frac{1}{2}\{\hat{v}_a, \hat{\mathcal{L}}^p\}$ and $\frac{1}{2}\{\hat{v}_a, \hat{s}^p\}$, respectively. Here, the matrix element of orbital angular momentum \mathcal{L} in the band representation reads (take $e = \hbar = 1$) [9, 13, 14, 26–28]

$$\mathcal{L}_{mn}(\mathbf{k}) = \frac{i}{4\mu_B} \sum_{\ell \neq m,n} \left(\frac{1}{\varepsilon_\ell - \varepsilon_m} + \frac{1}{\varepsilon_\ell - \varepsilon_n} \right) \mathbf{v}_{m\ell} \times \mathbf{v}_{\ell n}, \quad (2)$$

where μ_B is the Bohr magneton, ε_n is the band energy with n the band index, $\mathbf{v}_{\ell n}$ is the velocity matrix element, and the k -dependence of the band quantities is made implicit.

One can make the following observations. First, due to the band energy difference factors in the denominator, \mathcal{L} is significantly enhanced at band near-degeneracies. This suggests that topological metals, which have protected band degeneracies around Fermi level, could be good platforms to realize large NOHE. Second, nonzero \mathcal{L} as well as orbital Hall response does not require SOC. However, in nonmagnetic systems, SOC is essential for the spin current response, as nonzero matrix element of s requires spin-polarized bands. Third, the diverging factors in \mathcal{L} do not appear in s , implying that the orbital response may dominate over its spin counterpart around band near-degeneracies, even in the presence of strong SOC. Consider a band near-degeneracy with local gap $\Delta\varepsilon$, and $s \sim 1$ for fully spin polarized band. The orbital-spin ratio $\mathcal{L}/s \sim m_e v_F^2 / \Delta\varepsilon$, with v_F the characteristic velocity of the electrons. For typical value of $v_F \sim 10^6$

TABLE I. Symmetry-allowed nonlinear tensor components $\chi_{a(bc)}^a$ for the representative materials studied in this work. For the point group (PG) D_{3h} , the two-fold axis is taken along y .

Material	PG	Allowed $\chi_{a(bc)}^a$
RhSi	T	$\chi_{xyy}^x = \chi_{yzz}^y = \chi_{zxx}^z, \chi_{xzz}^x = \chi_{yxx}^y = \chi_{zyy}^z$
YPtBi	T_d	$\chi_{xyy}^x = \chi_{yzz}^y = \chi_{zxx}^z$ $= -\chi_{xzz}^x = -\chi_{yxx}^y = -\chi_{zyy}^z$
PbTaSe ₂	D_{3h}	$\chi_{y(xz)}^y$

m/s and relatively large $\Delta\varepsilon \sim 100$ meV, this ratio is already a few tens. This indicates the possible dominance of orbital response in topological metals, even for those having large SOC.

Intrinsic NOHE. The features observed above are general, regardless of specific microscopic mechanisms. Below, we shall focus on the intrinsic mechanism of NOHE, which represents an inherent property of each material, determined solely by the band structure.

Employing the extended semiclassical theory [29–32], which has been successfully applied in studying various nonlinear response effects, we obtain the following formula of response tensor for intrinsic NOHE (see Appendix):

$$\chi_{a(bc)}^p = \frac{1}{2} \int [d\mathbf{k}] \left[\Lambda_{abc,n}^p f_0 - \left(\langle j_a^p \rangle_n G_{bc,n} - \langle v_b \rangle_n \mathfrak{G}_{ac,n}^p - \langle v_c \rangle_n \mathfrak{G}_{ab,n}^p \right) f_0' \right], \quad (3)$$

where $[d\mathbf{k}]$ is a shorthand notation for $\sum_n d\mathbf{k}/(2\pi)^3$, f_0 is the Fermi distribution, $\langle v_a \rangle_n = \langle u_n | \hat{v}_a | u_n \rangle$ is the intraband velocity matrix element for band n , similar for $\langle j_a^p \rangle_n$. The tensors G , \mathfrak{G} , and Λ are respectively the Berry connection polarizability, orbital BCP, and orbital BCP dipole. Their detailed expressions are given in Appendix. Like Berry curvature, these quantities are band geometric properties, manifesting interband coherence.

To illustrate the general features, we first apply this formula to a Weyl point model:

$$\mathcal{H} = \frac{k^2}{2m} + \nu \mathbf{k} \cdot \boldsymbol{\sigma}, \quad (4)$$

where m is an effective mass, $\boldsymbol{\sigma}$ is the vector of Pauli matrices, and $\nu = \pm 1$ determines the chirality of the Weyl point at $k = 0$. This model permits a CP nonlinear orbital current j_z^z driving by applied E field in the x - y plane. Figure 1(a) shows the corresponding tensor component χ_{zxx}^z calculated as a function of chemical potential μ . One can see the NOHE response is peaked at the Weyl point energy, showing a significant enhancement by topological band degeneracy. In Fig. 1(b), we

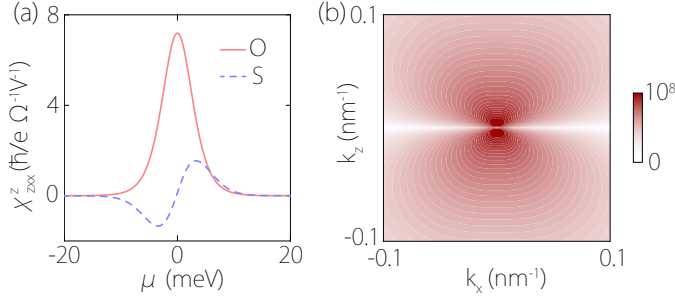


FIG. 1. Nonlinear CP orbital current response in Weyl model. (a) Calculated intrinsic NOHE conductivity χ_{zxx}^z (red curve) versus chemical potential μ . The blue dashed curve is for the corresponding nonlinear spin current response. (b) k -resolved contribution to χ_{zxx}^z for μ slightly above the Weyl point. The unit of color map is nm³/V. Here, we take $m = 1.2m_e$, $\nu = 1.0$ eV \cdot Å, and $T = 20$ K.

plot the k -resolved contribution (the integrand of (3)) to χ_{zxx}^z for μ slightly above the Weyl point, confirming the enhancement is indeed from Weyl electron states. For comparison, by taking σ in model (4) as spin, we also evaluate the nonlinear spin Hall conductivity, plotted as the dashed curve in Fig. 1(a). One observes that (i) although the spin response is also enhanced around the Weyl point, its magnitude is still much smaller than the orbital one (note the Weyl model is a model with strong SOC); (ii) the spin response exhibits a (resonance-like) line-shape different from the peak profile of orbital response. These results are consistent with the general features we argued above.

RhSi: weak SOC. Since NOHE does not require SOC, we first investigate it in a topological metal with weak SOC: RhSi, which has a chiral structure with T point group symmetry. Our calculation reveals it can produce a remarkable out-of-plane torque generated by NOHE, stronger than the linear out-of-plane spin-orbit torques reported so far.

The lattice structure of RhSi is shown in Fig. 2(a). The CP orbital Hall current is forbidden in linear response. However, according to Table I, it is allowed by NOHE, characterized by components $\chi_{zxx}^z = \chi_{xyy}^x = \chi_{yzz}^y$ and $\chi_{zyy}^z = \chi_{yxx}^y = \chi_{xzz}^x$ (the coordinate axis are marked in Fig. 2(a)). The calculated band structure of RhSi is plotted in Fig. 2(c), which is consistent with previous works [33, 34] (Calculation details are given in Supplementary Note 8). There are several band crossing points close to Fermi level. At the Γ point, there are two crossing points with twofold and fourfold degeneracy. Along high-symmetry paths, such as Γ -X and Γ -R, RhSi also host type-I and type-II Weyl points, as shown in Fig. 2(c). As we mentioned, such topological metal band structure is promising to trigger large NOHE.

Figure 2(d) shows the calculated χ_{zxx}^z of NOHE as a function of chemical potential at room temperature. For

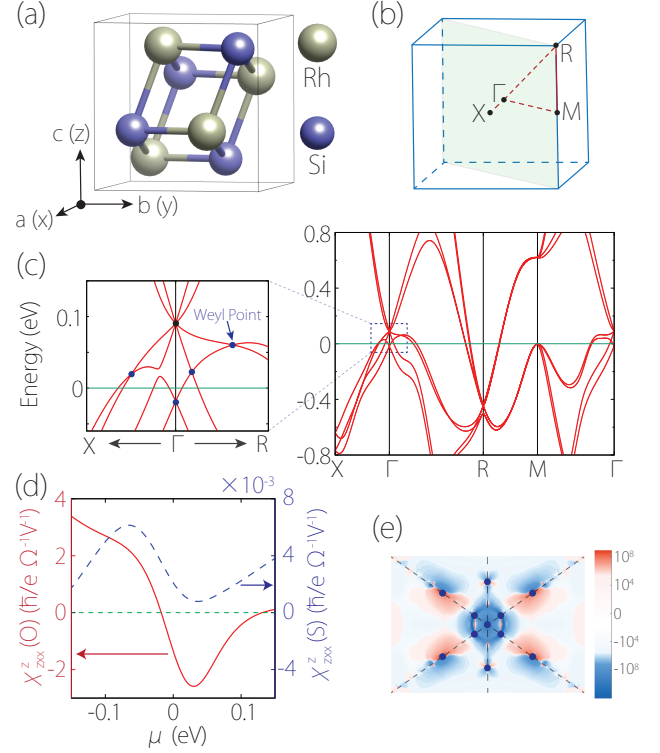


FIG. 2. (a) Lattice structure and (b) Brillouin zone of RhSi. (c) Calculated band structure with SOC. Left panel shows the enlarged view of the dashed box around Γ . (d) Calculated NOHE conductivity χ_{zxx}^z (O) (red curve) versus chemical potential at room temperature. The blue dashed curve is for the corresponding nonlinear spin current response χ_{zxx}^z (S). (e) k -resolved contributions to NOHE χ_{zxx}^z around the Γ point on the intrinsic Fermi level in Γ -M-R plane. The unit of color map is Å³/V.

comparison, the corresponding component of nonlinear spin Hall response is also evaluated (dashed line). One finds that the nonlinear orbital Hall conductivity is large $\sim -1.35 \hbar/e \Omega^{-1} \text{V}^{-1}$ at intrinsic Fermi level, and it is nearly three orders of magnitude larger than the spin response. To pinpoint the origin of this large nonlinear orbital response, we plot the k -resolved contribution to χ_{zxx}^z in Fig. 2(e), which shows significant contributions are coming from the regions around the band degeneracy points. These results demonstrate that the NOHE response is greatly enhanced by topological nodal features of RhSi.

To compare NOHE with previously reported linear spin and orbital Hall effects, it is convenient to convert χ into an effective linear out-of-plane orbital Hall conductivity, defined by $\sigma_{\text{OH}}^{\text{oop}} = \chi \rho j$, where j is the injected charge current density and ρ is the (linear) longitudinal resistivity of the material. Using the reported value $\rho \sim 3 \times 10^{-4} \Omega \text{ cm}$ for RhSi [35] and $j = 10^7 \text{ A/cm}^2$, we find $\sigma_{\text{OH}}^{\text{oop}} \sim -4050 \hbar/e \Omega^{-1} \text{cm}^{-1}$. Furthermore, in order for orbital current to produce a torque on a neighboring

TABLE II. Results of nonlinear CP orbital current and spin current responses for the representative topological semimetals. Calculated nonlinear orbital Hall conductivity (NOHC) and nonlinear spin Hall conductivity (NSHC) are in units of $\hbar/e \Omega^{-1}V^{-1}$. OHA and SHA denote the orbital Hall angle and spin Hall angle, respectively. And the last three lines are for the out-of-plane effective orbital Hall angle including the η factor, for $\eta = 2.91\%$ (Co), $\eta = -18\%$ (Gd) and $\eta = 38\%$ (Fe_3GaTe_2).

	RhSi	YPtBi	PbTaSe ₂
NOHC	-1.35	-1.58	-0.76
NSHC	0.0021	0.020	0.023
OHA	-2.44	-2.84	-3.63
SHA	0.0038	0.036	0.11
$\theta_{\text{OH}}^{\text{oop}} (\eta = 2.91\%)$	-0.071	-0.083	-0.11
$\theta_{\text{OH}}^{\text{oop}} (\eta = -18\%)$	0.44	0.51	0.65
$\theta_{\text{OH}}^{\text{oop}} (\eta = 38\%)$	-0.93	-1.08	-1.38

magnetic layer, the orbital moment has to be converted into spin moment after entering the magnetic layer, characterized by an orbital-to-spin conversion efficiency η . Thus, concerning the resulting torque, it is more meaningful to consider the combination $\eta\sigma_{\text{OH}}^{\text{oop}}$. For 3d ferromagnets, such as Fe, Co, CoFe, and Ni, η is positive and ranges from 0.92% to 4.55% [15]. More recent works found larger η in Gd ($\eta \sim -18\%$) [16] and Fe_3GaTe_2 ($\eta \sim 38\%$) [18]. For orbital torques exerted on these two materials, the value of $\eta\sigma_{\text{OH}}^{\text{oop}}$ can reach $729 \hbar/e \Omega^{-1}\text{cm}^{-1}$ and $-1539 \hbar/e \Omega^{-1}\text{cm}^{-1}$, respectively. Such values are much larger than the out-of-plane torques (using low-symmetry materials) reported to date, which are usually much less than $200 \hbar/e \Omega^{-1}\text{cm}^{-1}$ [36–42].

In addition, the torque efficiency is typically characterized by the effective orbital/spin Hall angle. It is defined as $\theta_{\text{OH}}^{\text{oop}} = \eta(2e/\hbar)\rho\sigma_{\text{OH}}^{\text{oop}}$ for NOHE, and it can reach 0.44 and -0.93 for RhSi to produce orbital torques on Gd and Fe_3GaTe_2 , respectively. These values are significantly larger than the ever reported strongest out-of-plane linear torque efficiencies, which range from 0.03 to 0.11 [37–41, 43].

YPtBi: strong SOC and switchable orbital torque.

Next, we consider a topological metal with strong SOC: YPtBi. We will see that NOHE still dominates over its spin counterpart, due to the enhancement from band degeneracy.

YPtBi has attracted wide interest for potential applications in superconductivity, thermoelectricity, and spintronics [44–46]. As shown in Fig. 3(a), it is a half-Heusler crystal with space group $F\bar{4}3m$ (No. 216). The calculated band structure of YPtBi is plotted in Fig. 3(b). It is semimetallic, with a fourfold Dirac point near the Fermi level at Γ . The result is consistent with previous studies [47].

The T_d point group symmetry of YPtBi forbids any

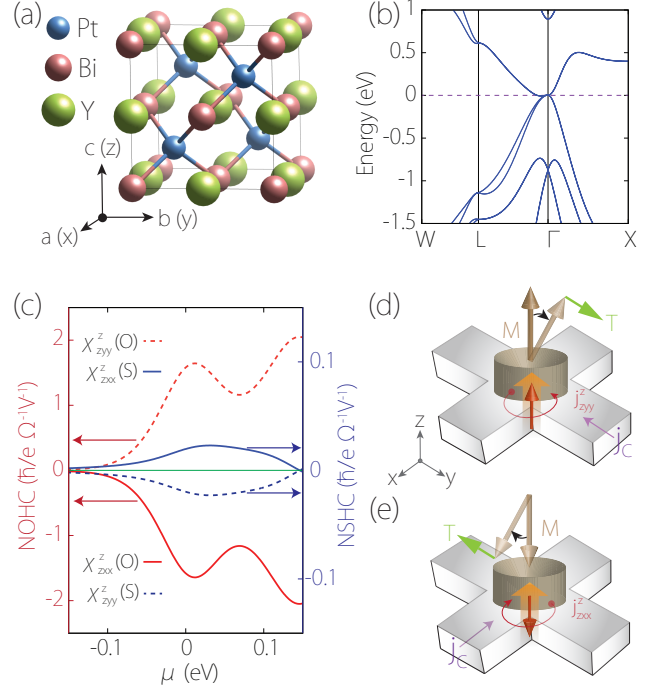


FIG. 3. Switchable CP NOHE in YPtBi. (a) Lattice structure of YPtBi. (b) Band structure with SOC included. (c) Calculated NOHE conductivities χ_{zxx}^z and χ_{zyy}^z (red curves) versus chemical potential at room temperature. The blue curves show the results for the corresponding nonlinear spin current responses. (d,e) Schematic figure for a bilayer device structure. The CP orbital current generated from NOHE in the bottom layer (and the resulting torque on the top magnetic layer) can be switched by controlling the driving current direction (in x or y direction).

CP orbital Hall current in linear response, but allows it at nonlinear order. To generate CP orbital current flowing along the z direction, the relevant conductivity components are $\chi_{zxx}^z = -\chi_{zyy}^z$. Figure 3(c) presents the calculated χ_{zxx}^z and χ_{zyy}^z . The corresponding nonlinear spin Hall conductivity components are also shown for comparison. One can see χ_{zxx}^z ($= -\chi_{zyy}^z$) exhibits a peak at intrinsic Fermi level, with a peak value of $-1.58 \hbar/e \Omega^{-1}V^{-1}$, manifesting the enhancement by degeneracy between conduction and valence bands. And the orbital response is still two order of magnitude larger than the spin response ($\sim 0.020 \hbar/e \Omega^{-1}V^{-1}$), despite the spin response is already amplified by the large SOC. These findings confirm the general features we argued above.

Using the experimentally measured resistivity $\rho \sim 3 \times 10^{-4} \Omega \text{ cm}$ at room temperature [44] and an injected current density $j = 10^7 \text{ A/cm}^2$, we estimate the corresponding effective linear out-of-plane orbital Hall conductivity $\sigma_{\text{OH}}^{\text{oop}} \sim -4740 \hbar/e \Omega^{-1}\text{cm}^{-1}$, which is even larger than that of RhSi.

For applications, it is desirable to have an easy con-

trol over the sign of generated torque. For NOHE, this cannot be done by simply reversing the sign of applied E field (or injected current). However, for YPtBi, because $\chi_{xxx}^z = -\chi_{zyy}^z$, the sign switching can be readily achieved by rotating the injected current direction by $\pi/2$. As illustrated in Figs. 3(d) and 3(e), the sign of the generated CP orbital current (and hence the orbital torque on the top ferromagnetic layer) is opposite between the two in-plane current directions. This offers a simple device setup to realize switchable orbital torques.

Discussion. We have proposed a strategy to achieve field-free deterministic switching of PMA magnets, using the orbital torques generated by NOHE. As a new physical effect, we find NOHE permits the generation of CP orbital current, a key ingredient for switching PMA magnets, in a large class of crystals, much beyond the scope allowed by linear response. Moreover, we have shown that NOHE is significantly enhanced by band near-degeneracies, around which it can dominate over the spin response by orders of magnitude, even in systems with strong SOC. So far, studies on orbital torques mostly focused on materials with weak SOC, such as the 3d transition metals. By harnessing the nonlinear mechanisms, our findings greatly broadens the material platforms for orbitronics.

Particularly, our results suggest topological metals as promising orbital source materials, due to the dramatic enhancement of nonlinear orbital response by the inter-band coherence associated with topological band degeneracies. Besides RhSi and YPtBi having nodal points in band structures, the similar feature is also manifested in nodal-line topological metals, such as PbTaSe₂ (see Table, details in Supplementary Note 5).

In the calculations, we focused on the intrinsic NOHE. At the level of relaxation time approximation, we obtain an extrinsic contribution to NOHE given by

$$\chi_{abc}^p = -\tau^2 \int [d\mathbf{k}] \partial_b f_0 \partial_c \langle j_a^p \rangle_n, \quad (5)$$

where τ is the relaxation time. We have computed this contribution and found it is subdominant compared to the intrinsic NOHE for the material example RhSi (see Supplementary Note 7). We note that although a systematic theory for the extrinsic NOHE remains to be developed, the general features, including the symmetry conditions, the enhancement by band near-degeneracies, and the comparison between orbital and spin responses, should hold for both intrinsic and extrinsic contributions.

* These authors contributed equally to this work.

† cong Xiao@fudan.edu.cn

‡ shengyuan.yang@polyu.edu.hk

§ ricky_ang@sutd.edu.sg

- [1] B. A. Bernevig, T. L. Hughes, and S.-C. Zhang, Orbitronics: The intrinsic orbital current in p-doped silicon, *Phys. Rev. Lett.* **95**, 066601 (2005).
- [2] G. Y. Guo, Y. Yao, and Q. Niu, Ab initio calculation of the intrinsic spin hall effect in semiconductors, *Phys. Rev. Lett.* **94**, 226601 (2005).
- [3] H. Kontani, T. Tanaka, D. Hirashima, K. Yamada, and J. Inoue, Giant orbital hall effect in transition metals: Origin of large spin and anomalous hall effects, *Phys. Rev. Lett.* **102**, 016601 (2009).
- [4] D. Go, D. Jo, C. Kim, and H.-W. Lee, Intrinsic spin and orbital hall effects from orbital texture, *Phys. Rev. Lett.* **121**, 086602 (2018).
- [5] D. Jo, D. Go, and H.-W. Lee, Gigantic intrinsic orbital hall effects in weakly spin-orbit coupled metals, *Phys. Rev. B* **98**, 214405 (2018).
- [6] S. Bhowal and S. Satpathy, Intrinsic orbital moment and prediction of a large orbital hall effect in two-dimensional transition metal dichalcogenides, *Phys. Rev. B* **101**, 121112 (2020).
- [7] G. Sala and P. Gambardella, Giant orbital hall effect and orbital-to-spin conversion in 3 d, 5 d, and 4 f metallic heterostructures, *Phys. Rev. Res.* **4**, 033037 (2022).
- [8] L. Salemi and P. M. Oppeneer, First-principles theory of intrinsic spin and orbital hall and nernst effects in metallic monoatomic crystals, *Phys. Rev. Mater.* **6**, 095001 (2022).
- [9] A. Pezo, D. García Ovalle, and A. Manchon, Orbital hall effect in crystals: Interatomic versus intra-atomic contributions, *Phys. Rev. B* **106**, 104414 (2022).
- [10] M. Costa, B. Focassio, L. M. Canonico, T. P. Cysne, G. R. Schleder, R. B. Muniz, A. Fazzio, and T. G. Rappoport, Connecting higher-order topology with the orbital hall effect in monolayers of transition metal dichalcogenides, *Phys. Rev. Lett.* **130**, 116204 (2023).
- [11] Y.-G. Choi, D. Jo, K.-H. Ko, D. Go, K.-H. Kim, H. G. Park, C. Kim, B.-C. Min, G.-M. Choi, and H.-W. Lee, Observation of the orbital hall effect in a light metal ti, *Nature* **619**, 52 (2023).
- [12] I. Lyalin, S. Alikhah, M. Berritta, P. M. Oppeneer, and R. K. Kawakami, Magneto-optical detection of the orbital hall effect in chromium, *Phys. Rev. Lett.* **131**, 156702 (2023).
- [13] B. Göbel and I. Mertig, Orbital hall effect accompanying quantum hall effect: Landau levels cause orbital polarized edge currents, *Phys. Rev. Lett.* **133**, 146301 (2024).
- [14] B. Göbel, L. Schimpf, and I. Mertig, Topological orbital hall effect caused by skyrmions and antiferromagnetic skyrmions, *Commun. Phys.* **8**, 17 (2025).
- [15] D. Lee, D. Go, H.-J. Park, W. Jeong, H.-W. Ko, D. Yun, D. Jo, S. Lee, G. Go, J. H. Oh, *et al.*, Orbital torque in magnetic bilayers, *Nat. Commun.* **12**, 6710 (2021).
- [16] S. Ding, M.-G. Kang, W. Legrand, and P. Gambardella, Orbital torque in rare-earth transition-metal ferrimagnets, *Phys. Rev. Lett.* **132**, 236702 (2024).
- [17] Y. Yang, P. Wang, J. Chen, D. Zhang, C. Pan, S. Hu, T. Wang, W. Yue, C. Chen, W. Jiang, *et al.*, Orbital torque switching in perpendicularly magnetized materials, *Nat. Commun.* **15**, 8645 (2024).
- [18] D. Zhang, H. Wei, J. Duan, J. Chen, J. Chen, D. Yue, W. Gong, P. Liu, Y. Yang, J. Gou, *et al.*, Orbital torque switching of room temperature two-dimensional van der waals ferromagnet fe3gate2, *Nat. Commun.* **16**, 7047 (2025).

- [19] A. Manchon, J. Železný, I. M. Miron, T. Jungwirth, J. Sinova, A. Thiaville, K. Garello, and P. Gambardella, Current-induced spin-orbit torques in ferromagnetic and antiferromagnetic systems, *Rev. Mod. Phys.* **91**, 035004 (2019).
- [20] J. Ryu, S. Lee, K.-J. Lee, and B.-G. Park, Current-induced spin-orbit torques for spintronic applications, *Adv. Mater.* **32**, 1907148 (2020).
- [21] I. M. Miron, K. Garello, G. Gaudin, P.-J. Zermatten, M. V. Costache, S. Auffret, S. Bandiera, B. Rodmacq, A. Schuhl, and P. Gambardella, Perpendicular switching of a single ferromagnetic layer induced by in-plane current injection, *Nature* **476**, 189 (2011).
- [22] L. Liu, O. J. Lee, T. J. Gudmundsen, D. C. Ralph, and R. A. Buhrman, Current-induced switching of perpendicularly magnetized magnetic layers using spin torque from the spin hall effect, *Phys. Rev. Lett.* **109**, 096602 (2012).
- [23] H. Kurebayashi, Going in the right direction, *Nat. Phys.* **13**, 209 (2017).
- [24] H. Yang and Y. Liu, Field-free and unconventional switching of perpendicular magnetization at room temperature, *Nat. Electron.* **6**, 724 (2023).
- [25] J. Sinova, S. O. Valenzuela, J. Wunderlich, C. H. Back, and T. Jungwirth, Spin hall effects, *Rev. Mod. Phys.* **87**, 1213 (2015).
- [26] Óscar Pozo Ocaña and I. Souza, Multipole theory of optical spatial dispersion in crystals, *SciPost Phys.* **14**, 118 (2023).
- [27] A. Pezo, D. García Ovalle, and A. Manchon, Orbital hall physics in two-dimensional dirac materials, *Phys. Rev. B* **108**, 075427 (2023).
- [28] O. Busch, I. Mertig, and B. Göbel, Orbital hall effect and orbital edge states caused by *s* electrons, *Phys. Rev. Res.* **5**, 043052 (2023).
- [29] Y. Gao, S. A. Yang, and Q. Niu, Field induced positional shift of bloch electrons and its dynamical implications, *Phys. Rev. Lett.* **112**, 166601 (2014).
- [30] Y. Gao, S. A. Yang, and Q. Niu, Geometrical effects in orbital magnetic susceptibility, *Phys. Rev. B* **91**, 214405 (2015).
- [31] Y. Gao, Semiclassical dynamics and nonlinear charge current, *Front. Phys.* **14**, 33404 (2019).
- [32] C. Xiao, Y. Ren, and B. Xiong, Adiabatically induced orbital magnetization, *Phys. Rev. B* **103**, 115432 (2021).
- [33] G. Chang, S.-Y. Xu, B. J. Wieder, D. S. Sanchez, S.-M. Huang, I. Belopolski, T.-R. Chang, S. Zhang, A. Bansil, H. Lin, and M. Z. Hasan, Unconventional chiral fermions and large topological fermi arcs in rhsi, *Phys. Rev. Lett.* **119**, 206401 (2017).
- [34] Z. Ni, B. Xu, M.-Á. Sánchez-Martínez, Y. Zhang, K. Manna, C. Bernhard, J. Venderbos, F. De Juan, C. Felser, A. G. Grushin, *et al.*, Linear and nonlinear optical responses in the chiral multifold semimetal rhsi, *npj Quantum Mater.* **5**, 96 (2020).
- [35] L. Z. Maulana, K. Manna, E. Uykur, C. Felser, M. Dressel, and A. V. Pronin, Optical conductivity of multifold fermions: The case of rhsi, *Phys. Rev. Res.* **2**, 023018 (2020).
- [36] D. MacNeill, G. Stiehl, M. Guimaraes, R. Buhrman, J. Park, and D. Ralph, Control of spin-orbit torques through crystal symmetry in wte2/ferromagnet bilayers, *Nat. Phys.* **13**, 300 (2017).
- [37] Y. Liu, G. Shi, D. Kumar, T. Kim, S. Shi, D. Yang, J. Zhang, C. Zhang, F. Wang, S. Yang, *et al.*, Field-free switching of perpendicular magnetization at room temperature using out-of-plane spins from tairte4, *Nat. Electron.* **6**, 732 (2023).
- [38] Y. Zhang, H. Xu, K. Jia, G. Lan, Z. Huang, B. He, C. He, Q. Shao, Y. Wang, M. Zhao, *et al.*, Room temperature field-free switching of perpendicular magnetization through spin-orbit torque originating from low-symmetry type ii weyl semimetal, *Sci. Adv.* **9**, eadg9819 (2023).
- [39] M. Dc, D.-F. Shao, V. D.-H. Hou, A. Vailionis, P. Quarterman, A. Habiboglu, M. Venuti, F. Xue, Y.-L. Huang, C.-M. Lee, *et al.*, Observation of anti-damping spin-orbit torques generated by in-plane and out-of-plane spin polarizations in mnpd3, *Nat. Mater.* **22**, 591 (2023).
- [40] L. Bainsla, B. Zhao, N. Behera, A. M. Hoque, L. Sjöström, A. Martinelli, M. Abdel-Hafez, J. Åkerman, and S. P. Dash, Large out-of-plane spin-orbit torque in topological weyl semimetal tairte4, *Nat. Commun.* **15**, 4649 (2024).
- [41] F. Wang, G. Shi, K.-W. Kim, H.-J. Park, J. G. Jang, H. R. Tan, M. Lin, Y. Liu, T. Kim, D. Yang, *et al.*, Field-free switching of perpendicular magnetization by two-dimensional ptte2/wte2 van der waals heterostructures with high spin hall conductivity, *Nat. Mater.* **23**, 768 (2024).
- [42] F. Han, J. Zhang, F. Yang, B. Li, Y. He, G. Li, Y. Chen, Q. Jiang, Y. Huang, H. Zhang, *et al.*, Generation of out-of-plane polarized spin current by non-uniform oxygen octahedral tilt/rotation, *Nat. Commun.* **15**, 7299 (2024).
- [43] I. Abdelwahab, D. Kumar, T. Bian, H. Zheng, H. Gao, F. Hu, A. McClelland, K. Leng, W. L. Wilson, J. Yin, *et al.*, Two-dimensional chiral perovskites with large spin hall angle and collinear spin hall conductivity, *Science* **385**, 311 (2024).
- [44] N. P. Butch, P. Syers, K. Kirshenbaum, A. P. Hope, and J. Paglione, Superconductivity in the topological semimetal yptbi, *Phys. Rev. B* **84**, 220504(R) (2011).
- [45] M. Goyal and M. Sinha, Effect of spin-orbital coupling on the electronic, mechanical, thermoelectric, and vibrational properties of xptbi (*x* = sc and y): A first-principles study, *J. Phys. Chem. Solids* **153**, 110024 (2021).
- [46] T. Shirokura, N. H. D. Khang, and P. N. Hai, High-efficient spin orbit torque generated by topological semimetal yptbi deposited on oxidized si substrates, *Appl. Phys. Lett.* **124**, 052402 (2024).
- [47] W. Feng, D. Xiao, Y. Zhang, and Y. Yao, Half-heusler topological insulators: A first-principles study with the tran-blaha modified becke-johnson density functional, *Phys. Rev. B* **82**, 235121 (2010).
- [48] L. Dong, C. Xiao, B. Xiong, and Q. Niu, Berry phase effects in dipole density and the mott relation, *Phys. Rev. Lett.* **124**, 066601 (2020).
- [49] H. Liu, J. Zhao, Y.-X. Huang, X. Feng, C. Xiao, W. Wu, S. Lai, W.-B. Gao, and S. A. Yang, Berry connection polarization tensor and third-order hall effect, *Phys. Rev. B* **105**, 045118 (2022).
- [50] C. Wang, Y. Gao, and D. Xiao, Intrinsic nonlinear hall effect in antiferromagnetic tetragonal cumnns, *Phys. Rev. Lett.* **127**, 277201 (2021).
- [51] H. Liu, J. Zhao, Y.-X. Huang, W. Wu, X.-L. Sheng, C. Xiao, and S. A. Yang, Intrinsic second-order anomalous hall effect and its application in compensated antiferromagnets, *Phys. Rev. Lett.* **127**, 277202 (2021).

- [52] S. Lai, H. Liu, Z. Zhang, J. Zhao, X. Feng, N. Wang, C. Tang, Y. Liu, K. Novoselov, S. A. Yang, *et al.*, Third-order nonlinear hall effect induced by the berry-connection polarizability tensor, *Nat. Nanotechnol.* **16**, 869 (2021).
- [53] A. Gao, Y.-F. Liu, J.-X. Qiu, B. Ghosh, T. V. Trevisan, Y. Onishi, C. Hu, T. Qian, H.-J. Tien, S.-W. Chen, M. Huang, D. Bérubé, H. Li, C. Tzschaschel, T. Dinh,

Z. Sun, S.-C. Ho, S.-W. Lien, B. Singh, K. Watanabe, T. Taniguchi, D. C. Bell, H. Lin, T.-R. Chang, C. R. Du, A. Bansil, L. Fu, N. Ni, P. P. Orth, Q. Ma, and S.-Y. Xu, Quantum metric nonlinear hall effect in a topological antiferromagnetic heterostructure, *Science* **381**, 181 (2023).

End Matter

Appendix: Formulae of intrinsic NOHE. The formulae for intrinsic NOHE can be obtained by the approach of extended semiclassical theory [29–32]. In this approach, the orbital current density is expressed as

$$j_a^p = \int [d\mathbf{k}] f_{n\mathbf{k}} \langle W_{n\mathbf{k}} | \hat{j}_a^p | W_{n\mathbf{k}} \rangle, \quad (\text{A1})$$

where $[d\mathbf{k}]$ is a shorthand notation for $\sum_n d\mathbf{k}/(2\pi)^3$ with n as the band index and \mathbf{k} the crystal momentum, the last factor is the orbital current carried by the wave packet $|W_{n\mathbf{k}}\rangle$ which in the absence of E field is centered at Bloch state $|u_{n\mathbf{k}}\rangle$, and $f_{n\mathbf{k}}$ is the distribution function. For an intrinsic response, we take Fermi-Dirac distribution for $f_{n\mathbf{k}}$, and the last factor in (A1) can be obtained from a variation of semiclassical action, as developed in Refs. [32, 48] and detailed in the Supplementary Note 3.

The intrinsic nonlinear orbital conductivity is obtained

to be

$$\chi_{a(bc)}^p = \frac{1}{2} \int [d\mathbf{k}] \left[\Lambda_{abc,n}^p f_0 - \left(\langle j_a^p \rangle_n G_{bc,n} - \langle v_b \rangle_n \mathfrak{G}_{ac,n}^p - \langle v_c \rangle_n \mathfrak{G}_{ab,n}^p \right) f_0' \right]. \quad (\text{A2})$$

Here, we suppressed the \mathbf{k} labels in the integrand, $f_0 \equiv f_0(\varepsilon_n)$ is the Fermi distribution with ε_n the unperturbed band energy; $\langle v_a \rangle_n = \langle u_n | \hat{v}_a | u_n \rangle$ is the intraband velocity matrix element, similar for $\langle j_a^p \rangle_n$. Besides,

$$G_{bc,n} = 2\text{Re} \sum_{\ell \neq n} \frac{\langle v_b \rangle_{n\ell} \langle v_c \rangle_{\ell n}}{(\varepsilon_n - \varepsilon_\ell)^3} \quad (\text{A3})$$

is known as the Berry connection polarizability (BCP) [29, 49], which already plays important roles in several nonlinear effects [50–53], and

$$\mathfrak{G}_{ac,n}^p = 2\text{Re} \sum_{\ell \neq n} \frac{\langle j_a^p \rangle_{n\ell} \langle v_c \rangle_{\ell n}}{(\varepsilon_n - \varepsilon_\ell)^3} \quad (\text{A4})$$

may be dubbed the orbital BCP. In the same sense,

$$\Lambda_{abc,n}^p = -2\text{Re} \sum_{m \neq n} \left[\frac{3 \langle v_b \rangle_{nm} \langle v_c \rangle_{mn} (\langle j_a^p \rangle_n - \langle j_a^p \rangle_m)}{(\varepsilon_n - \varepsilon_m)^4} - \frac{\langle \partial_b j_a^p \rangle_{nm} \langle v_c \rangle_{mn} + \langle \partial_c j_a^p \rangle_{nm} \langle v_b \rangle_{mn}}{(\varepsilon_n - \varepsilon_m)^3} \right. \\ \left. - \sum_{\ell \neq n} \frac{(\langle v_b \rangle_{\ell m} \langle v_c \rangle_{mn} + \langle v_c \rangle_{\ell m} \langle v_b \rangle_{mn}) \langle j_a^p \rangle_{n\ell}}{(\varepsilon_n - \varepsilon_\ell)(\varepsilon_n - \varepsilon_m)^3} - \sum_{\ell \neq m} \frac{(\langle v_b \rangle_{\ell n} \langle v_c \rangle_{nm} + \langle v_c \rangle_{\ell n} \langle v_b \rangle_{nm}) \langle j_a^p \rangle_{m\ell}}{(\varepsilon_m - \varepsilon_\ell)(\varepsilon_n - \varepsilon_m)^3} \right] \quad (\text{A5})$$

can be regarded as the orbital counterpart of BCP dipole

$\partial_a G_{bc}$, where $\partial_a \equiv \partial/\partial k_a$.